Journal of Fluorescence
https://doi.org/10.1007/s10895-024-03628-6

RESEARCH

Achieving White Light Emission with High Luminescence Efficiency via Combustion Produced $Sr_3Y(PO_4)_3$: Dy^{3+} Nanophosphors for Photonic Applications

Diksha Rani[1] · Anil Kumar[2] · Dinesh Kumar[1]

Received: 11 January 2024 / Accepted: 19 February 2024

Abstract
Extensive investigations were conducted on the structural and photoluminescence characteristics of the present nanosamples, encompassing PL, TEM, PXRD, EDAX, CCT, and CIE research. PXRD studies established a single phase, and TEM instruments were used to examine the dimensions and topographical behavior. The EDAX analysis examined the magnitude of the different components that were present. Decay lifetimes, radiative and non-radiative energy transfer rates, and a number of intensity limitations have all been found using PL spectra. Two significant peaks were visible in the blue (B) and yellow (Y) regions of the photoluminescence (PL) spectra upon NUV excitation, at 486 nm and 577 nm. At 7 mol% Dy^{3+} ions, the PL intensity peaked. After that, it began to decline as a result of the concentration quenching process brought on by multipolar exchanges (s = 4.1445). The values of 0.86423 ms, 81%, and 226 s^{-1} were discovered to be the decay life time, non radiative rates, and quantum efficiency of the ideal powder, respectively. Further analysis of $Sr_3Y_{0.93}Dy_{0.07}(PO_4)_3$ nanocrystals revealed that their chromaticity coordinates (0.305, 0.321), and CCT value (6902 K) matched those of NTSE and commercial LEDs, certifying their use in innovative optoelectronic appliances, particularly single phased WLEDs.

Keywords Photoluminescence characteristics · Topographical behavior · Intensity · Concentration quenching · Quantum efficiency

Introduction

Modern life is significantly influenced by light and light-based technologies, which has altered the quality of life. Rare-earth-activated nanocrystals are a significant class of solid state lightings (SSLs) that have attracted the attention of materials scientists. In comparison to conventional solid-state lighting sources like halogen tungsten lamp, incandescent light, fluorescent lamp, and so on, white light-emitting diodes (w-LEDs), in particular the phosphor converted w-LEDs, have a longer working lifetime, higher energy efficiency, better eco-friendliness, and faster response time. There are currently two methods that are quite popular for making w-LEDs. The first method involves coating a blue LED with a single-phased yellow emitting phosphor or coating a near ultra-violet (NUV) LED with a single-phased white emitting phosphor. However, due to shortcomings in the red spectral area, such w-LEDs are still unable to fulfill the best demand in the illumination sector, resulting in high color correlated temperature (CCT) and a less color rendering index (CRI). The second method involves coating a NUV LED with three distinct red-blue-green phosphors. Now a days, single phased emanating nanophosphor is chosen over RGB-based systems in certain circumstances due to the second method's high cost and complicated fabrication approach [1–8].

Dy^{3+} is one of the most alluring rare earth ions, and because of its exceptional optical, electrical, and magnetic properties, it is frequently employed in optoelectronic functional materials. Excellent dopant candidates include dysprosium trivalent (Dy^{3+}) ions with a $4f^9$ electronic configuration, which under UV irradiation efficiently emit yellow in a variety of matrixes. Two main emissions from Dy^{3+} ions can be seen in the blue and yellow zones, corresponding to the $^4F_{9/2} \rightarrow {}^6H_{13/2}$ and $^4F_{9/2} \rightarrow {}^6H_{15/2}$ transitions, respectively.

✉ Dinesh Kumar
dineshdalal8@rediffmail.com

[1] Department of Chemistry, Deenbandhu Chhotu Ram University of Science and Technology, Murthal, Sonepat 131039, India

[2] Department of Chemistry, A. I. Jat. H. M. College, Rohtak 124001, India

Published online: 08 March 2024

The immediate environment of the Dy^{3+} activated host has very little impact on the magnetic-dipole transition of $^4F_{9/2} \rightarrow {}^6H_{15/2}$. But the environment in the immediate vicinity can easily influence the electric dipole transition of $^4F_{9/2} \rightarrow {}^6H_{13/2}$ [9, 10]. As a result, by choosing or adjusting the host framework, it is feasible to fine-tune the white light emission of Dy^{3+}, specifically to alter the emission ratio of yellow to blue photons. Along with activator ions, the choice of host matrix must be taken into account. Aluminates, borate, nitrides, tungstate, and phosphates have all been used as hosts in the fabrication of various Dy^{3+} activated phosphors. But at this time, phosphate-based host series have several benefits, including inexpensive synthesis costs, good chemical stability, and low sintering temperatures [11]. With the aforementioned benefits of phosphate-based host matrixes in mind, the author chose $Sr_3Y(PO_4)_3$ (SYPO) as the inorganic host matrix. In earlier reports, Wang et al. investigated the photouminescent properties of Dy^{3+} doped $Sr_3Y(PO_4)_3$ [12]. $Sr_3Y(PO_4)_3$:Dy^{3+} was investigated by Woo Seo et al. for near-ultraviolet white light-emitting diodes [13]. The luminescent properties of Dy^{3+} and Eu^{3+}co-doped $Sr_3Y(PO_4)_3$ were examined by Ren et al. [14]. Wang et al. investigated the photoluminescence and energy-transfer of Tm^{3+} and Dy^{3+} co-doped $Sr_3Y(PO_4)_3$ [15]. The majority of investigations conducted on the current host have employed a long-term, high-temperature solid-state synthetic process. However, we have created Dy^{3+} activated $Sr_3Y(PO_4)_3$ nanophosphors using a straightforward, highly efficient and energy-saving solution combustion method that allows for a 1200°C temperature drop and a 3-h sintering period. The activator ions are efficiently dissolved in the host matrix without changing the crystal phase of produced nanosamples. In comparison to other high-temperature methods, solution combustion produces crystalline, better pure, and uniform products with a worthy yield at a lower temperature. This improves the fabricated nanophosphor's emission profile and broadens its application domain in a variety of lighting applications.

Dy^{3+} activated $Sr_3Y(PO_4)_3$ nanocrystals were fabricated using the solution combustion fabrication method for first time, which is a self-igniting, environmentally friendly, energy-efficient, simple, and quick process that uses urea as a fuel. Several approaches are used to characterize the generated nanophosphor. The purity of synthesized samples was studied using PXRD (powder X-ray diffraction) analysis. TEM (transmission electron microscopy) was employed to evaluate the surface topography and particle size of the produced nanopowder. EDAX (energy dispersive X-ray analysis) was used to analyze the prepared sample's elemental configuration and nanocrystalline nature. The emission and excitation regions were identified by examining photoluminescent characteristics. Moreover, using the PL (photoluminescence) decay curve as a guide, radiative rates, non-radiative rates and quantum efficiency were determined for the entire series. A strong white emission was detected by photoluminescence spectroscopy, and CIE colour coordinates support this finding. The information provided by all of the reported characterizations is crucial for the effective implementation of white-emitting Dy^{3+} activated $Sr_3Y(PO_4)_3$ nanomaterials for lasers, latent fingerprinting, bio-imaging, photovoltaic, and advanced optoelectronic applications.

Synthesis and Characterization

Nanophosphor Fabrication

$Sr_3Y_{1-x}(PO_4)_3$: xDy^{3+} ($x = 0.01$ to 0.15 mol) nanomaterials were produced in a safe and efficient manner using the SC (solution-combustion) method. Beginning components such as Strontium nitrate ($Sr(NO_3)_2$), Yttrium (III) nitrate hexahydrate ($Y(NO_3)_3.6H_2O$), Dysprosium (III) nitrate hydrate ($Dy(NO_3)_3.xH_2O$), Diammonium hydrogen phosphate ($(NH_4)_2HPO_4$), and Urea (NH_2CONH_2) are obtained from Sigma-Aldrich and have a high purity (99.999%). Prior to being heated on a hot plate for roughly 8–10 min, all of these beginning components are first allowed to dissolve in accordance with their stoichiometric ratio in a small quantity of solvent, such as deionized water. At the microscopic level, the generated solution was uniformly dissolved. The combination was specifically preheated to roughly 80°C, which allows the water that was loosely bound to evaporate and the gelled substance to burn evenly. After that, a muffle furnace set to 500°C for 15 min was connected to the glass beaker, causing an auto-limited combustion reaction to occur. Because urea accelerated the breakdown of metallic nitrates, a lot of heat was released along with gases including CO_2, N_2, and moisture, which eventually turned the solution in the glass into a lot of residue. It was brought down to the room temperature. The material produced exhibits remarkable crystallinity, which can be attributed to the substantial quantity of energy generated during the combustion process. The powder was then crushed and calcined by placing it in a silica crucible and heating it to 1200°C for three hours in a muffle furnace. After that, the manufactured material was allowed to come to room temperature and was once more finely milled into a powder. Following that, the resultant nanocrystalline powder was placed inside a desiccator and went through various characterization procedures [16, 17]. The methodical flow diagram illustrates the synthetic process used to create the aforementioned nanosamples in Fig. 1.

Characterization

A Rigaku Ultima IV Diffractometer (Japan) having $\lambda = 0.154$ nm was used to record PXRD outlines for the phase analysis of the synthesized nanophosphors. The measured

Fig. 1 An illustration of the process flow for making Dy^{3+} activated $Sr_3Y(PO_4)_3$ nanophosphor

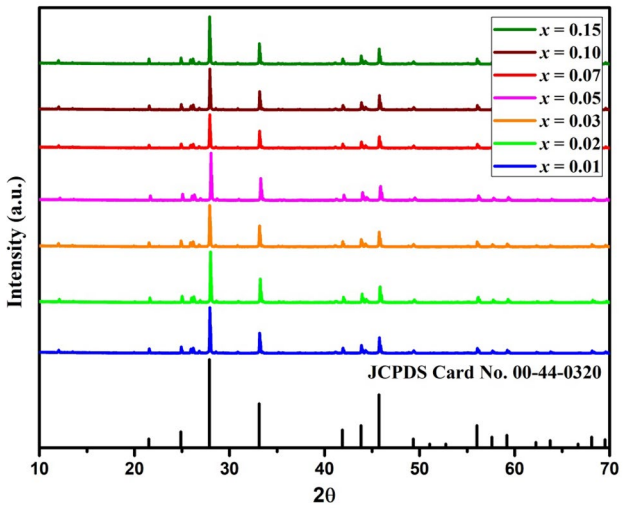

Fig. 2 The collective powder XRD patterns of Dy^{3+} activated $Sr_3Y(PO_4)_3$ exhibit perfect symbiosis with the standard host patterns

diffraction profiles of the produced samples are expressed as 2θ at a scan speed of 2° per minute (with an angular range of 10—70°). The TECNAI G2 FEI TEM technique was utilized to study the morphology and structure of nanocrystals. The presence of various components in nanocrystals was quantitatively evaluated using the Ametek (EDAX) technology. 15 kV and 11 mm were the operating power and distance settings, respectively. The Horiba-Jobin YVON Fluorolog Model FL-3–11 spectrophotometer, which is highly sophisticated and advanced, was utilized to investigate the attributes of photoluminescence, color compounds, and lifetime. The photomultiplier tube (PMT) voltage of 700 V and a slit width of 5 mm were used to trace the excitation and emission spectra. The CIE chromatic coordinate was computed using MATLAB software. Following extensive research, the superior optical performance of the $Sr_3Y_{0.93}Dy_{0.07}(PO_4)_3$ nanophosphors, which includes their high emission intensity and high quantum efficiency, makes them the preferred material for use in photonic devices, solar cells, WLEDs, bioimaging, sensors, and other applications [18].

Results and Discussion

PXRD Analysis

A diffractometer (Rigaku Ultima-IV) was used to gather the PXRD patterns of the $Sr_3Y_{1-x}(PO_4)_3$: xDy^{3+} ($x = 0.01$ to 0.15 mol) nanopowders within the 10—70° scan range. PXRD analysis was utilized to conclude the crystallographic investigations. The powder diffraction pattern (PDF) reference code: 00–44-0320 is found to be exactly identical to the recorded diffraction patterns related to the synthesized series of nanophosphors. The resulting patterns in addition to the host matrix standard patterns, which are shown in Fig. 2, show that doping trivalent dysprosium ions in the $Sr_3Y(PO_4)_3$ matrix does not change the phase prototype. The claimed standard diffraction pattern of the host and the experimental diffraction patterns for the activated system are identical. Because of their similar oxidation state and ionic radii, the efficient substitution of Y^{3+} (ionic radii = 1.01 Å) ions by activator ions raises the possibility of successful doping of Dy^{3+} (ionic radii = 0.91 Å) ions in $Sr_3Y(PO_4)_3$ host lattice. As a result, Dy^{3+} ions fit nicely in the $Sr_3Y(PO_4)_3$ host matrix and effectively substitute Y^{3+} ions. Still, a shift in peak intensities is noted, and this essentially depends on how the crystalline diffraction plane is oriented. In the event that there is a particular alignment, the intensity of the peak will be strong; in the event that the particles are placed in a disordered or random order, the peak's strength will be low. The radius percentage difference (Δ_r) could be calculated using the following equation to investigate the substitution mechanism [19, 20].

$$\Delta_r = \frac{R_m(CN) - R_d(CN)}{R_m(CN)} \times 100\% \quad (1)$$

In Eq. (1), CN stands for the coordination number, although R_d and R_m indicate the radii of the activator and host ions respectively. The ionic radii of cations are: Y^{3+} ($R_m = 1.01$ Å), Sr^{2+} ($R_m = 1.13$ Å) and doped ion Dy^{3+} ($R_d = 0.91$ Å). The determined radius percentage difference (Δ_r) value for the pair

Y^{3+} and Dy^{3+} is 9.9% and 19.47% for the pair Sr^{2+} and Dy^{3+}. The radius percentage difference in case of Y^{3+} is less as compared to Sr^{2+}. So, Dy^{3+} ions may occupy the position of the Y^{3+} ion. Secondly, the cations that are most likely to be replaced by the Dy^{3+} ion could be Sr^{2+} and La^{3+} both. But Dy^{3+} ions would take up the position of the Y^{3+} ion since both Y and Dy are in the trivalent oxidation state. Dy^{3+} will not replace Sr^{2+} because it results in a chemically non-equivalent replacement and adds an extra positive charge to the host lattice.

The average crystallite size of the nanosamples is evaluated using Scherrer's formula by estimating the crystallite size using full width at half maxima (FWHM) related to many strong XRD peaks. The equation for Debye Scherrer is provided below [21].

$$D = \frac{0.941\lambda}{\beta cos\theta} \tag{2}$$

In Eq. (2), the X-Ray wavelength (1.541 Å) is reported by λ, the diffraction angle is reported by θ, and the FWHM is implied by β. Using the aforementioned parameters, the generated nanophosphors series ($Sr_3Y_{1-x}(PO_4)_3$: xDy^{3+} (x = 0.01 to 0.15 mol)) has an average extent value of D which lies between 35 and 42 nm. Additionally, the following equations are used to compute the strain (ε) and dislocation density (δ) [22, 23].

$$\varepsilon = \frac{\beta cos\theta}{4} \tag{3}$$

$$\delta = \frac{1}{D^2} \tag{4}$$

The outcomes derived from the aforementioned equations are listed in the Table 1.

Morphological Analysis

TEM was used to evaluate the grain size and surface morphological characteristics of the synthesized nanosamples.

Table 1 The crystal size, dislocation density, and strain parameters of $Sr_3Y_{1-x}(PO_4)_3$: xDy^{3+} (x = 0.01 to 0.15 mol) nanophosphors

Sr. No.	Dy^{3+} Concentration (mol)	FWHM (β in degree)	D (nm)	δ (nm^{-2})	ε (strain)
1	0.01	0.201	42.6	0.00055	0.0035
2	0.02	0.217	39.4	0.00064	0.0038
3	0.03	0.225	38.0	0.00069	0.0039
4	0.05	0.234	36.6	0.00075	0.0041
5	0.07	0.241	35.5	0.00080	0.0042
6	0.10	0.236	36.2	0.00076	0.0041
7	0.15	0.228	37.5	0.00071	0.0040

A TEM image of $Sr_3Y_{0.93}Dy_{0.07}(PO_4)_3$ phosphor that has been calcined at 1200°C is seen in Fig. 3. The TEM image demonstrated the crystalline nature of the manufactured $Sr_3Y_{0.93}Dy_{0.07}(PO_4)_3$ powder, with particles located in the nanoscale (1–100 nm), reliable with the XRD findings. The grain size calculated through TEM is ~ 38 nm. Figure 4 shows the elemental estimation of the $Sr_3Y_{0.93}Dy_{0.07}(PO_4)_3$ (optimal sample), which was obtained via the EDAX investigation. The elements strontium (Sr), yttrium (Y), dysprosium (Dy), phosphorus (P), and oxygen (O) are indicated by the EDAX examination. The presence of these components alone confirmed successful doping with Dy^{3+} ions in the host matrix $Sr_3Y(PO_4)_3$.

Optical Analysis

Photoluminescence (PL) excitation and emission spectra are used to examine the photoluminescence performance of Dy^{3+} ions in $Sr_3Y(PO_4)_3$: Dy^{3+} nanophosphors. The PL-excitation spectrum of the representative sample $Sr_3Y_{0.93}Dy_{0.07}(PO_4)_3$ over the 300–500 nm spectral range is shown in Fig. 5. A type of powerful excitation peaks have been identified at 327, 352, 366, 389, 431, 457, and 472 nm corresponds to $^6H_{15/2} \rightarrow {}^6P_{3/2}$, $^6H_{15/2} \rightarrow {}^6P_{7/2}$, $^6H_{15/2} \rightarrow {}^6P_{5/2}$, $^6H_{15/2} \rightarrow {}^4I_{13/2}$, $^6H_{15/2} \rightarrow {}^4G_{11/2}$, $^6H_{15/2} \rightarrow {}^4I_{15/2}$ and $^6H_{15/2} \rightarrow {}^4F_{9/2}$ respectively, which masks the emission areas of blue and UV LED chips that are sold commercially. Consequently, their permissible use in nUV-triggered wLEDs is reflected in their abundant intense absorption in the near UV domain [24]. The excitation spectrum of Dy^{3+} ions revealed that the distinctive f-f transitions originated from the $^6H_{15/2}$ ground state. Figure 6 displays the emission spectra of all produced materials, which are identical in shape except

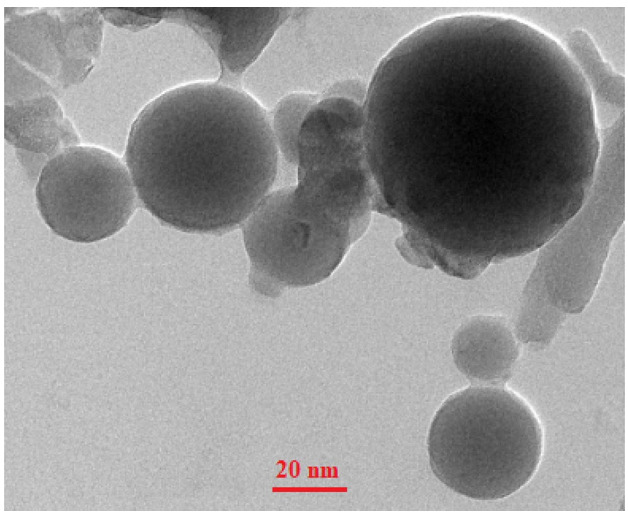

Fig. 3 TEM micrograph of $Sr_3Y_{0.93}Dy_{0.07}(PO_4)_3$ nanophosphor representing the surface morphology of the prepared nanosample

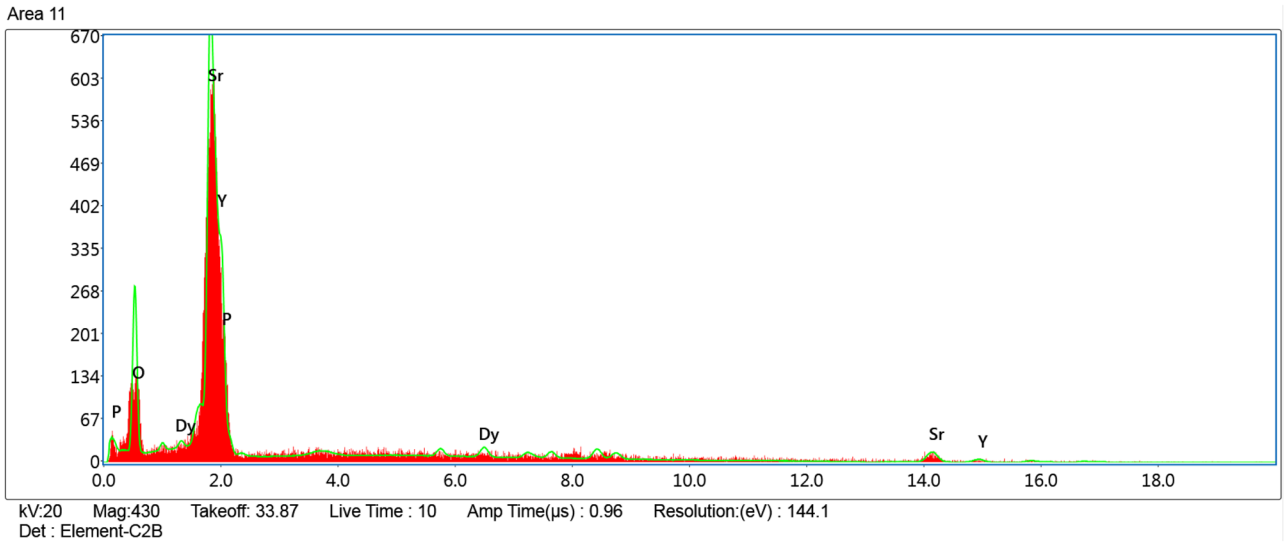

Fig. 4 EDAX study of $Sr_3Y_{0.93}Dy_{0.07}(PO_4)_3$, an optimal nanophosphor

their photoluminescence intensity. The emission spectrum is recorded at excitation wavelength 350 nm. Two prominent peaks were seen in the blue and yellow regions of the spectrum at 486 and 577 nm, respectively, which were subjected to the $^4F_{9/2} \rightarrow {}^6H_{15/2}$ and $^4F_{9/2} \rightarrow {}^6H_{13/2}$ transitions. Therefore, a mixture of yellow and blue light could produce white light. High symmetry locations in the host lattice containing Dy^{3+} ions were indicated by the magnetic dipole type of the notable $^4F_{9/2} \rightarrow {}^6H_{15/2}$ transition [25].

Moreover, White-light emission depends on the proper photoluminescence intensity, or Y/B (yellow to blue emission) ratio. The Y/B ratio is a quantitative measure of the asymmetry integral that takes into account the relative emission of the two prominent transitions of the dysprosium doped nanophosphor having stimulated wavelength 350 nm. The ratio of Y to B is calculated using the following formula [1, 26].

$$\frac{Y}{B} = \frac{\int_{550}^{600} I_2(\lambda)d\lambda}{\int_{450}^{500} I_1(\lambda)d\lambda} \tag{5}$$

It is discovered that as the concentration of Dy^{3+} ions varies, the Y/B ratio remains almost constant. Whereas the transition causing yellow emission at 577 nm ($^4F_{9/2} \rightarrow {}^6H_{13/2}$) is an electric dipole one that depends on the environment of crystal field, the one causing blue emission at 486 nm ($^4F_{9/2} \rightarrow {}^6H_{15/2}$) is a magnetic dipole change. The magnetic-dipole type of the significant $^4F_{9/2} \rightarrow {}^6H_{15/2}$ transition, however, suggests that dopant ions might be present at high symmetry sites in the lattice.

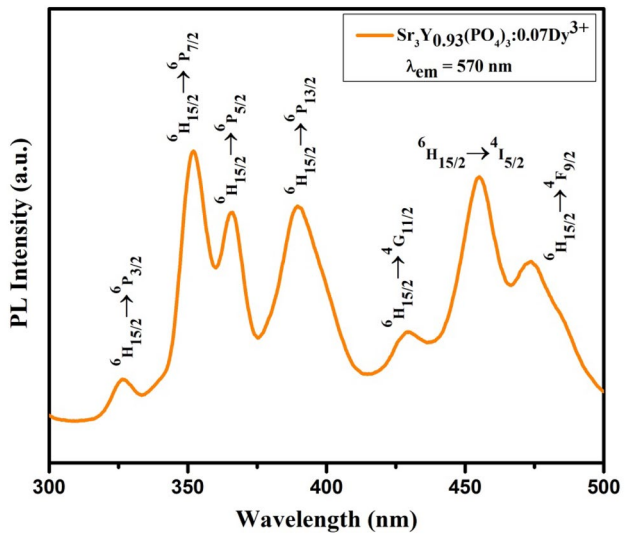

Fig. 5 Photoluminescent excitation spectra of $Sr_3Y_{0.93}Dy_{0.07}(PO_4)_3$ nanophosphor recorded at $\lambda_{em} = 570$ nm

Energy-Transfer Process

Figure 7 further illustrates the relationship between luminescence intensity and dopant content, showing that the PL emission intensity of manufactured nanophosphors increased as the concentration of Dy^{3+} ions increased up to 7 mol%, after which it started to decrease. This might be the result of the concentration scavenging phenomena, which happened as a result of non-radiative energy loss and has a variety of potential sources, including exchange communication, radiative reabsorption, and multipolar exchanges. There is a slim probability of radiative reabsorption occurring because

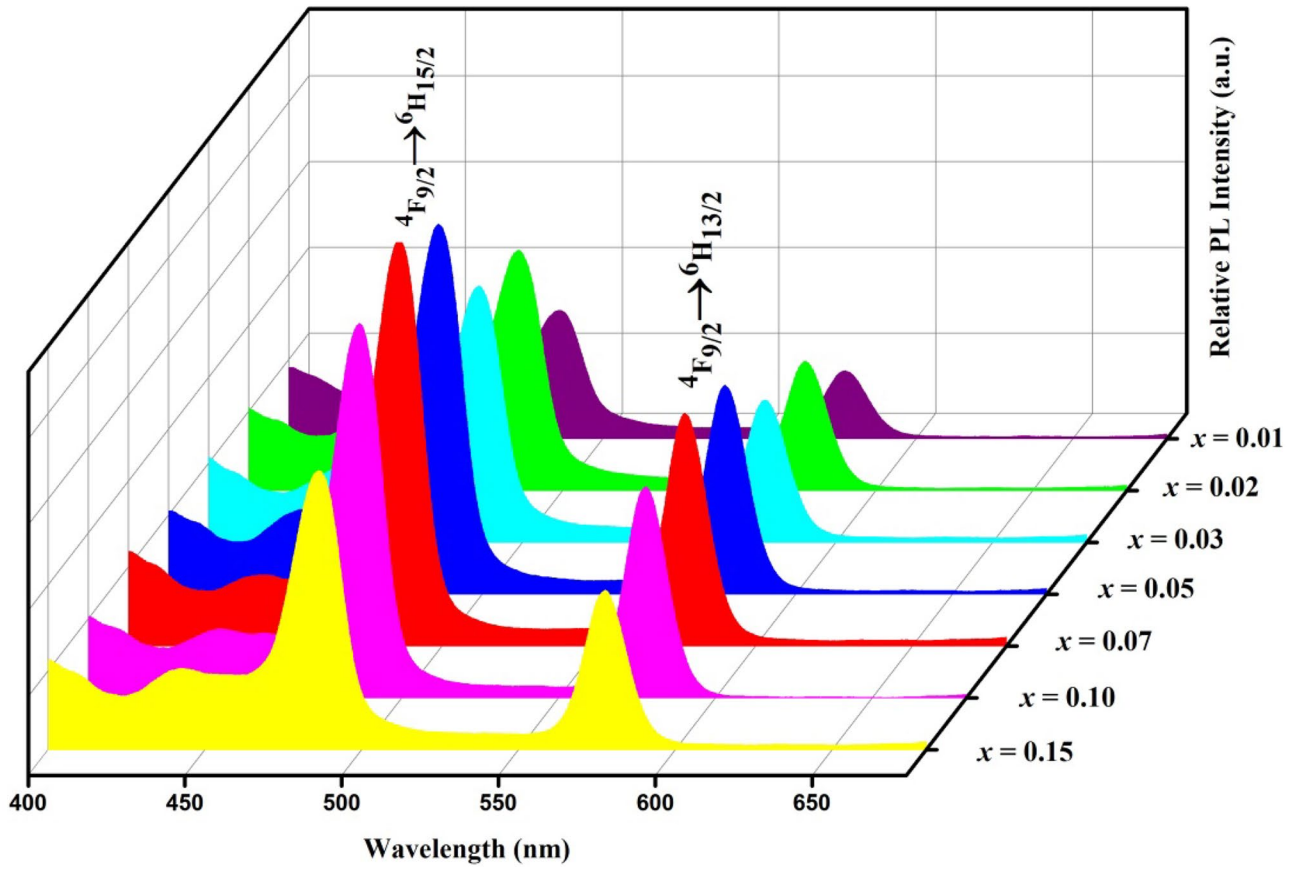

Fig. 6 Photoluminescent emission spectra of the series of Dy^{3+} activated $Sr_3Y(PO_4)_3$ nanophosphors recorded at $\lambda_{ex} = 350$ nm

there was no gurgling seen in the PL spectra. A critical distance of 4 Å must not be exceeded for energy exchange to occur between activator ions. The critical distance can be determined using Blasse's formulation in the manner shown below to confirm this [27].

$$R_c = 2\left[\frac{3V}{4\pi x_c N}\right]^{1/3} \tag{6}$$

where N is the number of cations living in a single unit cell, V denotes the volume of the unit cell, and x denotes the dopant composition for which the PL intensity is highest. Based on these values, the Rc was determined to be 19 Å, which is far greater than the recognized critical distance required for the exchange mechanism to occur. Multipolar exchanges, which might be dipole–dipole, dipole–quadrupole, or quadrupole–quadrupole in type, may therefore be the most widely recognised process for concentration scavenging. Dexter's formulation can be used to confirm the kind of exchanges that are actually occurring in the particular scenario, as follows [28]:

$$log\left(\frac{I}{x}\right) = log(f) - \left(\frac{s}{d}\right)logx \tag{7}$$

where d denotes the nanosample dimension, which in this case is 3, the ratio of emission intensity to activator ion

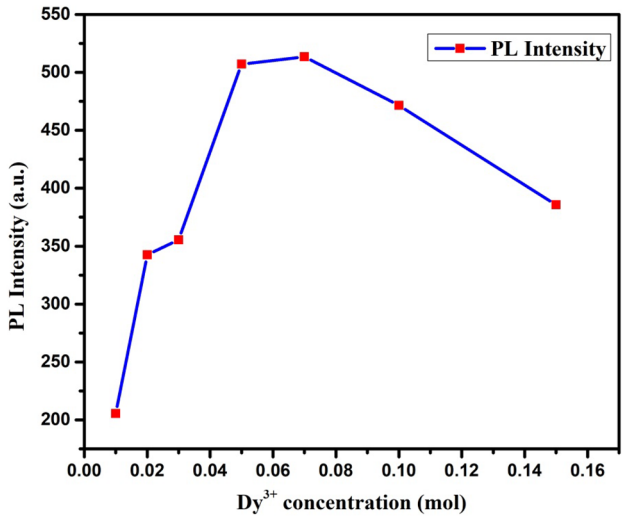

Fig. 7 Variation of the emission intensity at $\lambda_{ex} = 350$ nm as a function of Dy^{3+} concentration in nanophosphors

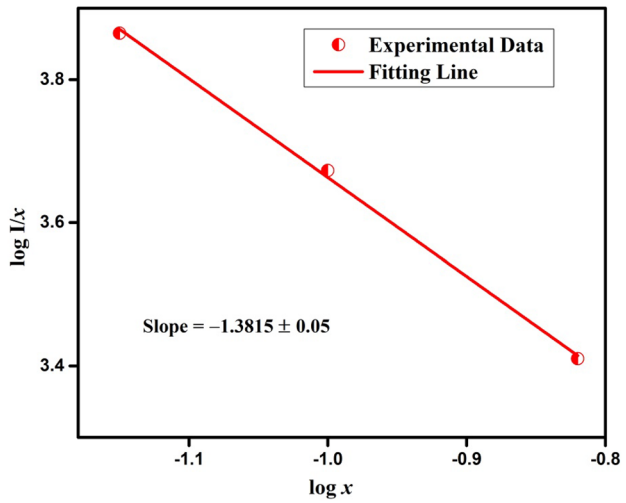

Fig. 8 A linear variation of log(I/x) with log(x) in Dy^{3+} activated $Sr_3Y(PO_4)_3$ nanophosphor

content is represented by the symbol I/x., and s is a constant with values of 6, 8, and 10 for d-d, d-q, and q-q interactions, respectively. A straight line with a slope of -1.3815 ± 0.05 is produced when log(I/x) and log(x) are plotted (as displayed in Fig. 8). This line yields the values of s = 4.1445, demonstrating the presence of multipolar exchanges that are in charge of the concentration quenching. Figure outlining in detail the many types of transitions associated with the excitation and emission phenomena for Dy^{3+} activated $Sr_3Y(PO_4)_3$ nanophosphors (as shown in Fig. 9).

Lifetime Decay

The decay profile of $Sr_3Y_{1-x}(PO_4)_3$: $xDy.^{3+}$ ($x = 0.01$ to 0.15 mol) nanocrystals is analyzed for the emission transition observed at 570 nm and excitation transition observed at 350 nm in order to further analyze the energy transfer behavior. Figure 10 displays the photoluminescence decay curves, which fit well with a 1st-order exponential decay mode. Mathematically, the 1st-order exponential decay equation is represented as [29]

$$I = I_0 e^{-t/\tau} \tag{8}$$

where I and I_0 are the photoluminescence intensities at time t and 0, respectively, and τ is the decay time. The first decay curve's exponential character indicates that the dopant ions are uniformly distributed throughout the host matrix. Figure 11 shows how the observed lifetimes in the $Sr_3Y(PO_4)_3$ host lattice vary with varying Dy^{3+} doping concentrations. As the concentration of activator ions rises from 0.01 mol to 0.15 mol, Table 2 and Fig. 11 clearly show a linear decrease in the average life expectancies from 1.03119 to 0.69022 ms. This can be explained by the non-radiative energy transmission that occurs between the different energy states of the activator ions. Apart from the fluorescence lifetime values

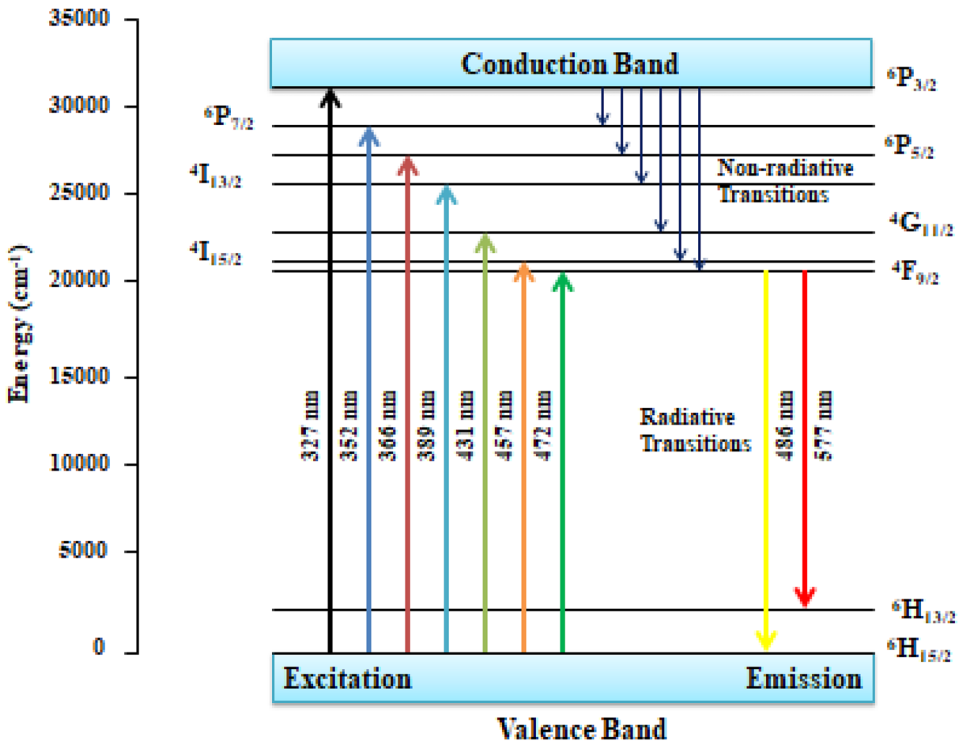

Fig. 9 Descriptive energy level diagram displaying various electronic transitions in different energy levels for the Dy^{3+} activated $Sr_3Y(PO_4)_3$ nanophosphors

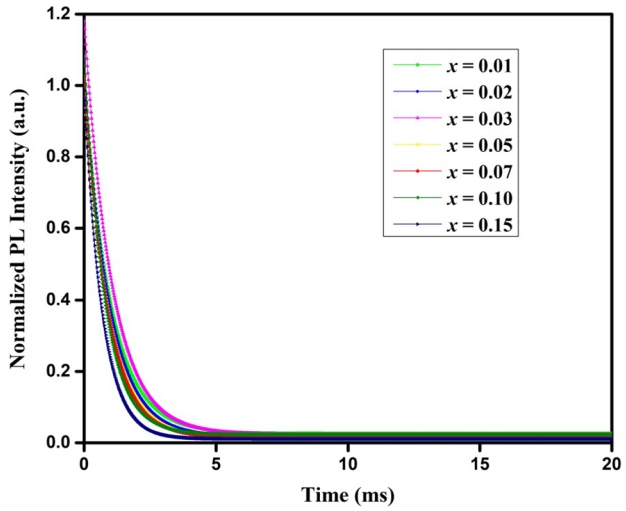

Fig. 10 Lifetime decay profile for the emission of Dy^{3+} activated $Sr_3Y(PO_4)_3$ nanophosphors recorded at $\lambda_{em} = 570$ nm and $\lambda_{ex} = 350$ nm

(measured in milliseconds) for the nanophosphor series, the auzel's model provides an explanation for the relationship that reveals the dependency of the obtained lifetime values on the concentration of Dy^{3+} ions [30].

$$\tau_c = \frac{\tau_R}{1 + \frac{c}{c_0} e^{-\frac{N}{3}}} \tag{9}$$

where τ_c is the decay lifespan at a concentration of c, N is the phonon number, and c_0 is the concentration constant. Aforementioned calculation is used to fit the experimentally evaluated PL lifespan data, and the resulting figures are displayed in Fig. 11. The fitting curve is signified by the solid black line, while the experimental data is shown by the pink round-shaped points. As can be seen in figure, the fitting curve derived from equation fits the experimental data quite well. During the fitting procedure, the value of N is found to be 8.016 ± 0.21, indicating that the quenching of the $^4F_{9/2}$ level through non-radiative relaxation results in the generation of about 8 phonons.

Additionally, based on Auzel's model, the intrinsic radiative lifetime (τ_R) for the $^4F_{9/2}$ level is determined to be 1.074 ± 0.04 ms. This information is then used to use the following equation to calculate the quantum efficiencies (φ) of the nanophosphor series.

$$\varphi = \frac{\tau_0}{\tau_R} = \frac{A_R}{A_R + A_{nR}} \tag{10}$$

In this case, the radiative and nonradiative rates of relaxation are represented by A_R and A_{nR}, respectively, and the measured average and intrinsic lifespan values (in ms) by τ_o and τ_R. Furthermore, by utilizing the τ_o and τ_R values in the given expression, the nonradiative relaxation rate A_{nR} (in s^{-1}) can be computed as follows [31].

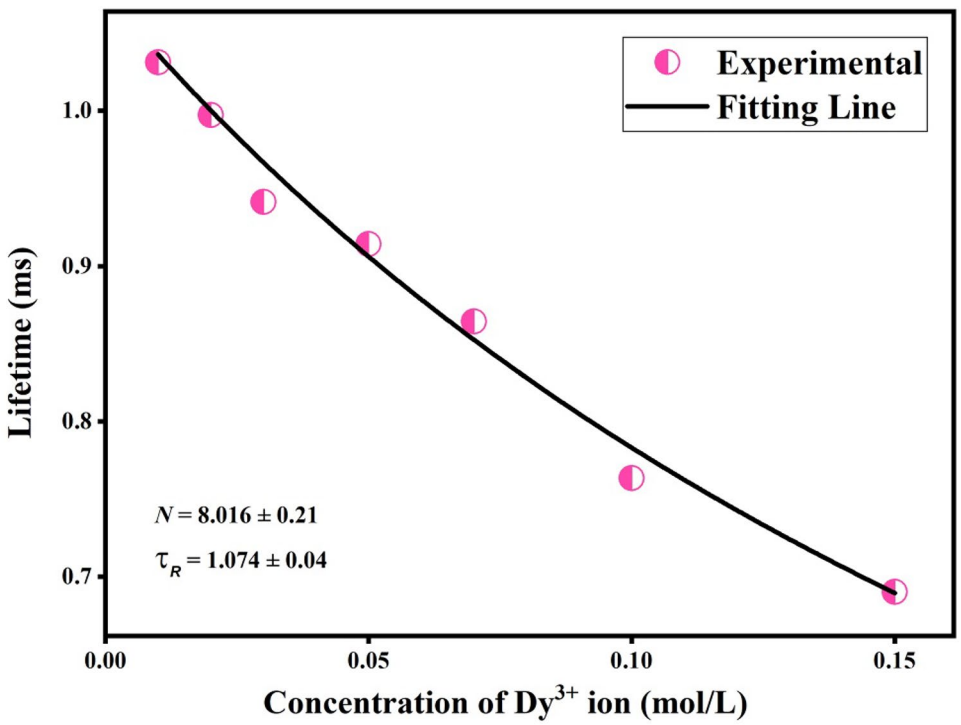

Fig. 11 Variation of decay lifetime with the doping concentration of Dy^{3+} ions using Auzel's formulation

Table 2 The Y/B ratio, lifetime decay values, non-radiative relaxation rates and quantum efficiencies of $Sr_3Y_{1-x}(PO_4)_3$: xDy^{3+} ($x = 0.01$ to 0.15 mol) nanophosphors

Sr. No.	Dy^{3+} Concentration (mol)	Y/B ratio	Lifetime (ms)	Non radiative rates (s^{-1})	Quantum efficiency (ϕ) (%)
1	0.01	0.548	1.03119	38	96
2	0.02	0.551	0.99730	71	93
3	0.03	0.566	0.94130	131	88
4	0.05	0.572	0.91429	162	86
5	0.07	0.574	0.86423	226	81
6	0.10	0.561	0.76346	378	71
7	0.15	0.552	0.69022	517	65

$$A_{nR} = \frac{1}{\tau_0} - \frac{1}{\tau_R} \tag{11}$$

As a result, Table 2 presents estimated values for the non-radiative rates and quantum efficiencies for the entire series of Dy^{3+} activated $Sr_3Y(PO_4)_3$ nanophosphors. Our nanophosphor sample $Sr_3Y_{0.93}Dy_{0.07}(PO_4)_3$ has a considerable quantum efficiency of approximately 81% for the optimum mol% doped composition, indicating its efficient use in solid-state lighting (SSL) devices and displays.

Chromaticity Coordinates and CCT

MATLAB software was used to analyze the color of the light produced from the created lighting nanopowders i.e.

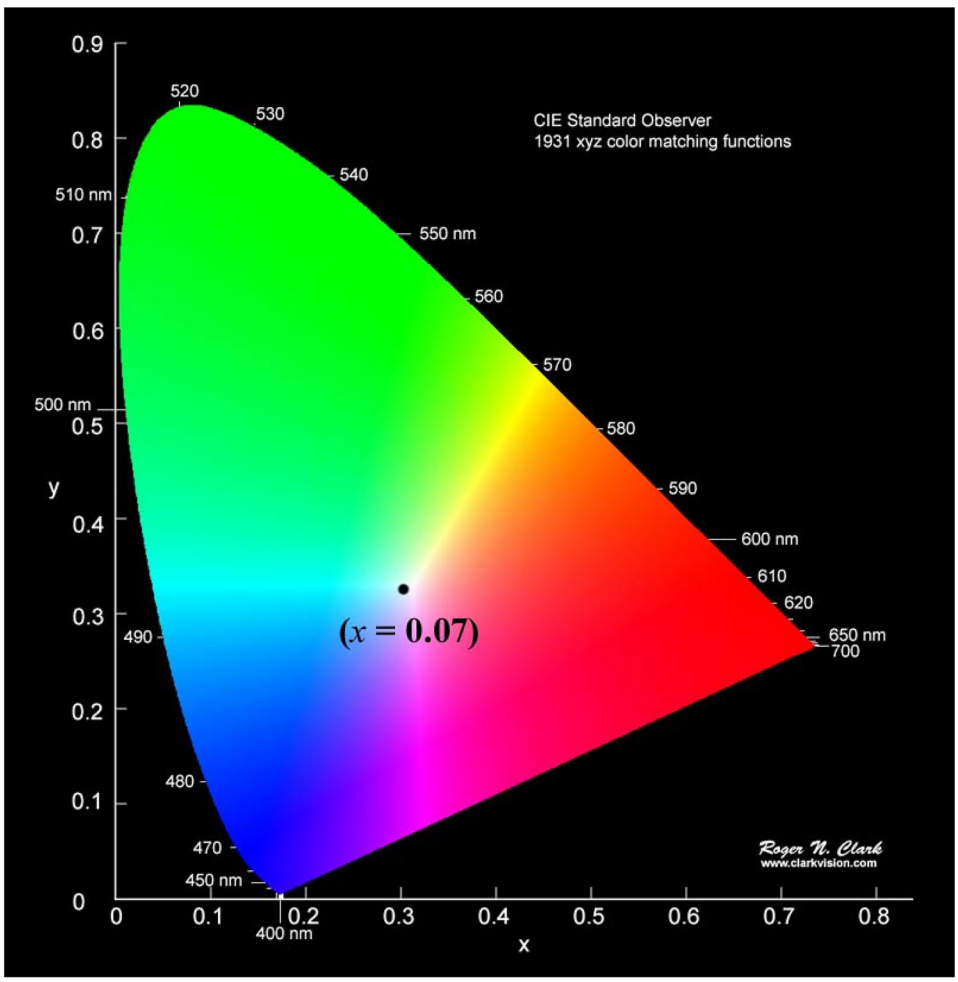

Fig. 12 CIE chromaticity diagram for optimal i.e. $Sr_3Y_{0.93}Dy_{0.07}(PO_4)_3$ nanophosphors

Table 3 CIE 1931 color co-ordinates, (u', v') and CCT values for $Sr_3Y_{1-x}(PO_4)_3$: xDy^{3+} ($x = 0.01$ to 0.15 mol) nanophosphors

Sr. No.	Dy^{3+} Concentration (mol)	Color Co-ordinates (x, y)	(u', v')	CCT (K)
1	0.01	(0.310, 0.324)	(0.198, 0.465)	6617
2	0.02	(0.299, 0.318)	(0.191, 0.457)	7256
3	0.03	(0.312, 0.314)	(0.199, 0.451)	6595
4	0.05	(0.308, 0.326)	(0.196, 0.468)	6701
5	0.07	(0.305, 0.321)	(0.195, 0.461)	6902
6	0.10	(0.309, 0.323)	(0.197, 0.464)	6674
7	0.15	(0.311, 0.319)	(0.198, 0.458)	6607

$Sr_3Y_{1-x}(PO_4)_3$: xDy^{3+} ($x = 0.01$ to 0.15 mol). The result of optimum concentration was certified by displaying the analyzed chromaticity coordinates in the CIE diagram (Fig. 12). The observed color coordinates are listed in Table 3. It was discovered that these values resembled the coordinates of the NTSE (National Television System Committee) and the commercial LEDs, which are (0.310, 0.316) and (0.320, 0.320), respectively.

Furthermore, in order to investigate the characteristics of the white light emitted, correlated color temperature (CCT) values were computed. These values show the temperature-based nature of the light, indicating its coolness (CCT ≥ 4000 K) and warmth (CCT ≤ 3200 K). Additionally, the CCT values are measured using the Mc-Camy relation as stated below [32].

$$CCT = -437n^3 + 3601n^2 - 6861n + 5514.31 \quad (12)$$

where x and y are the co-ordinates of the provided samples, and x_e and y_e are the chromaticity epicenter co-ordinates (0.332 and 0.186). In this case, n is the ratio between $x\text{-}x_e$ and $y\text{-}y_e$. The equation given below is also used to investigate a substantial partition of facets such as u' & v' coordinates [33];

$$u' = \frac{4x}{-2x + 12y + 3} \quad (13)$$

$$v' = \frac{9y}{-2x + 12y + 3} \quad (14)$$

As a result, the computed values of CCT are listed in Table 3 along with the u' and v' coordinates. For the $Sr_3Y_{1-x}(PO_4)_3$: xDy^{3+} ($x = 0.01$ to 0.15 mol) nanosample, the accumulated CCT values are observed to be more than 4000 K, confirming the fruitful use of the synthesized nanophosphors via solution-combustion methodology as an excellent source for the emission of cool white light in single-phased lights.

Conclusion

This work describes the effective creation of a series $Sr_3Y_{1-x}(PO_4)_3$: xDy^{3+} ($x = 0.01$ to 0.15 mol) nanophosphors using urea assisted combustion, a non-hazardous and environmentally friendly method, following sintering at 1200°C. A single phase with nearly no impurities was revealed by XRD examination of these nanophosphors. The nano-sized grains were revealed by TEM micrograph of the optimal nanopowder ($Sr_3Y_{0.93}Dy_{0.07}(PO_4)_3$) phosphor. An examination of the morphology revealed the irregularly clumped particles, measuring between 35 and 42 nm. SAED analysis is used to determine the polycrystalline nature, while EDAX study is used to confirm the elemental composition. White light was manifested by as-synthesized nanopowders, which displayed a blue (486 nm) and yellow (577 nm) band lead by 350 nm illumination. 7 mol% is found to be the ideal composition of trivalent dysprosium ions. There were multipolar exchanges that controlled the ability of phosphor powders to quench light. The single decay function conduct was represented by the decay curves, which also yielded the following results (for $Sr_3Y_{0.93}Dy_{0.07}(PO_4)_3$): decay time of 0.86423 ms, quantum efficiency of 81%, and non-radiative rate of 226 s^{-1}. The CIE 1931 coordinates of white light ($x = 0.305$, $y = 0.321$), along with the CCT value i.e. 6902 K, suggest that $Sr_3Y_{0.93}Dy_{0.07}(PO_4)_3$ is a superfine material that emits cool white light and is ideal for portable electronics, NUV-activated WLEDs, signage, aircraft cabins, digital communication, sensors, horticulture, advanced lasers, and solar cells.

Acknowledgements The authors are highly thankful to the department of chemistry, Deenbandhu Chhotu Ram University of Science and Technology, Murthal, Sonepat for providing the essential chemicals and instrumental services.

Author Contributions DR: Data analysis, original draft writing, Conceptualization and Methodology. AK: Reviewing and Editing. DK: Results discussion, Investigation and Supervision.

Funding The author, Diksha Rani, whole-heartedly acknowledges the University Grants Commission, India for receiving financial support in the form of JRF (NTA Ref. No. 191620241880).

Dinesh Kumar: Results discussion, Investigation and Supervision.

Data Availability No datasets were generated or analysed during the current study.

Declarations

Ethics Approval The research work presented in this paper is new and has not been published in any other journal. We will follow all norms of the publications like copyright etc.

Consent to Participate Not applicable.

Consent to Publish Not applicable.

Competing Interests The authors declare no competing interests.

References

1. Rani D, Kumar A, Kumar D (2023) Cool White – light Emanation Via Combustion Produced Sr 3 La (PO 4) 3: Dy 3 + single – phased Nanophosphors for Effective Lighting devices. J Fluoresc. https://doi.org/10.1007/s10895-023-03540-5
2. min Chen S, Zeng Q, Yao C et al (2022) Synthesis and luminescent properties of novel Li1.0Nb0.6Ti0.5O3: Dy3 + phosphors for white light-emitting diodes. J Lumin 244:118697. https://doi.org/10.1016/j.jlumin.2021.118697
3. Sehrawat P, Khatkar A, Boora P et al (2020) Fabrication of single-phase BaLaAlO 4: Dy nanophosphors by combustion synthesis. Mater Manuf Process 00:1–9. https://doi.org/10.1080/10426914.2020.1762206
4. Jacob LA, Sisira S, Mani KP et al (2020) High purity blue photoluminescence in thulium activated α-Na3Y(VO4)2 nanocrystals via host sensitization. J Lumin 223:117169. https://doi.org/10.1016/j.jlumin.2020.117169
5. Zhang Y, Liang Z, Wang W et al (2022) Optical properties of yellow-emitting Sr3LaNb3O12:Dy3 + phosphors with an abnormal thermal quenching for white light-emitting diode applications. J Mater Sci Mater Electron 33:26619–26632. https://doi.org/10.1007/s10854-022-09374-4
6. Slimi S, Loiko P, Bogdanov K et al (2022) Structure and luminescent properties of Dy3 + activated NaLa9(SiO4)6O2 yellow-emitting phosphors for application in white LEDs. J Alloys Compd 896:163109. https://doi.org/10.1016/j.jallcom.2021.163109
7. Dalal A, Nehra K, Hooda A et al (2022) Preparation and photoluminescent characteristics of green tb(III) complexes with β-diketones and N donor auxiliary ligands. Inorg Chem Commun 139:109349. https://doi.org/10.1016/j.inoche.2022.109349
8. Dahiya H, Dalal M, Siwach A et al (2020) A blue to green tunable Ba3GdP3O12:Tb3 + nanophosphor: structural and opto-electronic analysis. J Mater Sci Mater Electron 31:3750–3758. https://doi.org/10.1007/s10854-019-02009-1
9. Sehrawat P, Khatkar A, Boora P et al (2020) Emanating cool white light emission from novel down-converted SrLaAlO 4: Dy 3 + nanophosphors for advanced optoelectronic applications. Ceram Int 46:16274–16284. https://doi.org/10.1016/j.ceramint.2020.03.184
10. Kumar P, Singh S, Gupta I et al (2023) Structural and luminescent behaviour of Dy (III) activated Gd 3 Al 5 O 12 nanophosphors for white-LEDs applications. Mater Chem Phys 295:127035. https://doi.org/10.1016/j.matchemphys.2022.127035
11. Siwach A, Kumar D (2021) Structural and optical behavior of nano-scaled luminous green-emitting Ca9Y(PO4)7:Tb3 + phosphor for competent lighting devices. Chem Phys Lett 772:2–10. https://doi.org/10.1016/j.cplett.2021.138547
12. Wang J, Wang J, Duan P (2013) Luminescent properties of Dy3 + doped Sr3Y(PO 4)3 for white LEDs. Mater Lett 107:96–98. https://doi.org/10.1016/j.matlet.2013.06.001
13. Woo Seo Y, Heum Park S, Hyoung Chang S et al (2017) Tunable single-phased white-emitting Sr3Y(PO4)3:Dy3 + phosphors for near-ultraviolet white light-emitting diodes. Ceram Int 43:8497–8501. https://doi.org/10.1016/j.ceramint.2017.03.205
14. Ren Q, Wang B, Wu X et al (2016) Luminescence properties and energy transfer in Dy3 + and Eu3 + co-doped Sr3Y(PO4)3 phosphor. J Alloys Compd 684:677–682. https://doi.org/10.1016/j.jallcom.2016.05.141
15. Wang J, Wang J, Duan P (2014) Luminescence and energy transfer of Tm3 + or/and Dy3 + co-doped in Sr3Y(PO4)3 phosphors with UV excitation for WLEDs. J Lumin 145:1–5. https://doi.org/10.1016/j.jlumin.2013.07.014
16. Dahiya H, Dalal M, Dalal J et al (2018) Synthesis and luminescent properties of Tb3 + doped BaLa2ZnO5 nanoparticles. Mater Res Bull 99:86–92. https://doi.org/10.1016/j.materresbull.2017.11.005
17. Dalal M, Chahar S, Dalal J et al (2018) Energy transfer and photoluminescent analysis of a novel color-tunable Ba2Y1-xV3O11:xSm3 + nanophosphor for single-phased phosphor-converted white LEDs. Ceram Int 44:10531–10538. https://doi.org/10.1016/j.ceramint.2018.03.073
18. Devi P, Sehrawat P, Dalal H et al (2023) Exploring the orange – red emission from novel vanadate-based nanomaterials for highly innovative photonic applications. Bull Mater Sci. https://doi.org/10.1007/s12034-023-02938-y
19. Sehrawat P, Khatkar A, Devi S et al (2019) An effective emission of characteristic cool white light from Dy3 + doped perovskite type SrLa2Al2O7 nanophosphors in single-phase pc WLEDs. Chem Phys Lett 737:136842. https://doi.org/10.1016/j.cplett.2019.136842
20. Sheoran M, Sehrawat P, Kumari N et al (2021) Cool white light emanation and photo physical features of combustion derived Dy3 + doped ternary yttrate oxide based nanophosphors for down converted WLEDs. Chem Phys Lett 773:138608. https://doi.org/10.1016/j.cplett.2021.138608
21. Siwach A, Dalal M, Dahiya M, Kumar D (2020) Ca 9 Gd (PO 4) 7: sm 3 + — a novel single – phased down converting orange – red – emitting nanophosphor. J Mater Sci Mater Electron 31:13796–13807. https://doi.org/10.1007/s10854-020-03940-4
22. Dahiya M, Kumar D (2021) Single phase cool white light emitting novel Ca9Al(PO4)7:Dy3 + nanophosphor under NUV excitation. J Mater Sci Mater Electron 32:17241–17252. https://doi.org/10.1007/s10854-021-06201-0
23. Dahiya M, Siwach A, Dalal M, Kumar D (2021) Study of structural and luminescent characteristics of novel color tunable blue-green Tb3+-doped Na3Y(PO4)2 nanoparticles for NUV-based WLEDs. J Mater Sci Mater Electron 32:4166–4176. https://doi.org/10.1007/s10854-020-05158-w
24. Kumar BS, Umamahesvari H, Thyagarajan K et al (2023) Structural and photoluminescence properties of Dy3+-doped KMgBO3 phosphors. J Mater Sci Mater Electron 34:1–9. https://doi.org/10.1007/s10854-023-09974-8
25. Gupta I, Singh S, Kumar P et al (2022) Structural, morphological and optoelectronic aspects of YAlO3:Dy3 + doped nanocrystalline materials for NUV energized WLEDs. Curr Appl Phys 43:78–89. https://doi.org/10.1016/j.cap.2022.08.011
26. Dahiya H, Dalal M, Siwach A et al (2018) Cool white light emitting Ba5Zn4Y8O21:Dy3 + nanophosphors for single-phased WLEDs. J Mater Sci Mater Electron 29:20750–20758. https://doi.org/10.1007/s10854-018-0216-5

27. Devi P, Sehrawat P, Dalal H et al (2023) Crystal Phase Refinement and Optical features of highly efficient green light radiating ca 9 Y (VO 4) 7: Er 3 + nanophosphors for emerging solid-state lighting applications. J Fluoresc. https://doi.org/10.1007/s10895-023-03356-3
28. Devi P, Sehrawat P, Sheoran M et al (2023) Probing the Judd Ofelt parameters and photometric attributes of Eu 3 + - activated ca 9 Y (VO 4) 7 nanomaterials for emerging lighting applications. J Mater Sci Mater Electron 34:1–15. https://doi.org/10.1007/s10854-023-10264-6
29. Dalal H, Kumar M, Devi S et al (2023) Combustion Synthesis and Study of double charge transfer in highly efficient cool White-emitting Dy3 + activated vanadate-based Nanophosphor for Advanced Solid-state lighting. J Fluoresc 33:497–508. https://doi.org/10.1007/s10895-022-03098-8
30. Sehrawat P, Malik RK, Punia R, Maken S (2021) Optimizing the highly efficient cool-white luminescence via modulating Dy3 + ion into novel Sr6Al4Y2O15 nanocrystals for white LEDs. J Mater Sci Mater Electron 32:23486–23499. https://doi.org/10.1007/s10854-021-06837-y
31. Siwach A, Kumar D (2021) Structural and spectroscopic investigation of a novel orange-red Ca9Bi(PO4)7:Sm3 + nano-scaled phosphor. Solid State Sci 114:106528. https://doi.org/10.1016/j.solidstatesciences.2020.106528
32. Dalal H, Kumar M, Sehrawat P et al (2022) Crystallographic and photophysical aspects of combustion derived novel Dy3+-activated BaSrGd4O8 nanophosphor for advanced solid-state lighting applications. J Mater Sci Mater Electron 33:13743–13756. https://doi.org/10.1007/s10854-022-08307-5
33. Dahiya H, Siwach A, Dahiya M et al (2020) Structural and photoluminescence examination of red emissive Eu3+-doped nanophosphor synthesized via solution-combustion method. Chem Phys Lett 754:137657. https://doi.org/10.1016/j.cplett.2020.137657